Effective elastic properties of randomly fractured solids: 3D numerical experiments

E.H. Saenger, O.S. Krüger, and S.A. Shapiro

email: *saenger@geophysik.fu-berlin.de*

keywords: *effective velocities, scattering attenuation, finite differences, numerical rock physics*

ABSTRACT

This paper is concerned with numerical tests of several rock physical relationships. The focus is on effective velocities and scattering attenuation in 3D fractured media. We apply the so-called rotated staggered finite difference grid (RSG) technique for numerical experiments. Using this modified grid it is possible to simulate the propagation of elastic waves in a 3D medium containing cracks, pores or free surfaces without hard-coded boundary conditions. We simulate the propagation of plane waves through a set of randomly cracked 3D media. In these numerical experiments we vary the number and the distribution of cracks. The synthetic results are compared with several (most popular) theories predicting the effective elastic properties of fractured materials. We find that for randomly distributed and randomly oriented non-intersecting thin penny-shaped dry cracks the numerical simulations of P- and S- wave velocities are in good agreement with the predictions of the self-consistent approximation. We observe similar results for fluid-filled cracks. The standard Gassmann-equation cannot be applied to our 3D fractured media although we have a very low porosity in our models. This is well explained by the absence of a connected porosity. There is only a slight difference of effective velocities between the case of intersecting and non-intersecting cracks. This can be clearly demonstrated up to a crack density which is close to the connectivity percolation threshold. For crack densities beyond this threshold we observe that the differential effective medium (DEM) theory have the best fit with numerical results for intersecting cracks. Additionally it is shown that the scattering attenuation coefficient (of the meanfield) predicted by the classical Hudson-approach is in an excellent agreement with our numerical results.

INTRODUCTION

Discovering accurate relationships between pore structure and elastic properties of porous rocks is a long standing problem in geophysics, material science, and solid mechanics. Understanding the interaction between rock, pore space and fluids and how they control rock properties is crucial to a better understanding of acoustic and seismic data.

A range of different effective-medium theories (see Mavko et al. (1998) and references therein) give expressions for the overall properties of fractured media if the wavelength is large compared with the size of inclusions. There is a general agreement of those theories for a dilute concentration of inclusions. However, there are considerable differences for higher concentrations. Therefore, it is necessary to validate the different analytical predictions with experimental (e.g. Hudson et al. (2001)) or numerical data.

With this in mind Saenger and Shapiro (2002) presented an efficient and accurate way of finite-difference (FD) computer simulations of wave propagation and effective elastic properties in 2D fractured media. The present paper is a continuation of this work to three dimensional fractured media.

Spring network techniques (e.g. Garboczi and Day (1995); Garboczi and Berryman (2001); Ursenbach (2001)) are an alternative numerical method to study elastic moduli of porous media. All these methods are currently restricted to isotropic materials where the Poisson ratio cannot be chosen arbitrary. Attenua-

tion effects also cannot be described with these methods, because they treat the static case.
Finite difference (FD) methods discretize the wave equation on a grid. They replace spatial derivatives by FD operators using neighboring points. This discretization causes instability problems on a staggered grid (Virieux, 1986) when the medium contains high contrast discontinuities (strong heterogeneities). These difficulties can be avoided by using the rotated staggered grid (RSG) technique (Saenger et al., 2000). Since the FD approach is based on the wave equation without physical approximations, the method accounts not only for direct waves, primary reflected waves, and multiply reflected waves, but also for surface waves, head waves, converted reflected waves, and diffracted waves observed in ray-theoretical shadow zones (Kelly et al., 1976). Additionally, it accounts for the proper relative amplitudes. Consequently, we use this numerical method for our considerations of 3D fractured materials.
This paper is splitted in two main parts. First, we review several theoretical predictions of effective elastic properties of fractured media. In the second part we numerically validate the predictions. We explain our simulation setup with a detailed estimation of sources of errors and discuss the numerical results.

THEORIES OF EFFECTIVE PROPERTIES IN 3D FRACTURED MEDIA

In this paper we consider wave propagation through a well defined fractured region with thin penny-shaped cracks of equal form and size. For penny-shaped cracks (ellipsoidals with two major axis of equal size) one has to distinguish between cracks with non-zero aspect ratio α and an aspect ratio equal zero. The latter are refered to as disks. The commonly used crack density parameter ρ to characterize fractured materials is (Kachanov, 1992):

$$\rho = \frac{1}{V_0} N a^3 \tag{1}$$

where N is the total number of cracks, V_0 is the representative volume element and a is the radius of the penny-shaped cracks. The porosity is:

$$\phi = \frac{4}{3}\pi \frac{N}{V_0} a^2 d \tag{2}$$

with a and d as major axis (= radius) and minor axis of ellipsoid, respectively. If all cracks have the same ellipsoidal shape the relation between porosity ϕ and crack density ρ is (Cheng, 1993):

$$\phi = \frac{4}{3}\pi \alpha \rho \tag{3}$$

with $\alpha = d/a$ as the aspect ratio of penny-shaped ellipsoidal cracks.

Effective moduli of 3D fractured media with non-intersecting thin penny-shaped dry cracks

To describe wave propagation in fractured media we consider four different theories for thin dry penny shaped cracks in 3D-media, namely, the “Kuster-Toksöz formulation”, the “Self-Consistent approximation”, the “Differential Effective Medium (DEM) theory” and the “Theory for non-interacting cracks”. They can be used to predict effective wave velocities in the long wavelength approximation in dependency on porosity ϕ or crack density ρ. A detailed review of these rock physical relationships can be found in Mavko et al. (1998). Our goal is to investigate their limit of applicability for relatively high crack densities. Therefore, in order to compare our numerical results with these four theories we give here their respective effective bulk modulus $K^*(\phi)$ or effective Young’s modulus $E^*(\phi)$ and effective shear modulus $\mu^*(\phi)$. For the case of penny-shaped dry cracks with aspect-ratio α one can obtain the following formulae where K_m, E_m and μ_m are the bulk modulus, Young’s modulus and the shear modulus, respectively, of the homogeneous embedding.
Kuster and Toksöz (1974) derived expressions for effective elastic properties using a long wavelength first order scattering theory. They are formally limited to low porosity:

$$(K^*(\phi) - K_m)\frac{K_m + \frac{4}{3}\mu_m}{K^*(\phi) + \frac{4}{3}\mu_m} = -\phi K_m P_m, \tag{4}$$

$$(\mu^*(\phi) - \mu_m)\frac{\mu_m + \zeta_m}{\mu^*(\phi) + \zeta_m} = -\phi \mu_m Q_m. \tag{5}$$

with:

$$P_m = \frac{K_m}{\pi\alpha\beta_m}, \tag{6}$$

$$Q_m = \frac{1}{5} * \left[1 + \frac{8\mu_m}{\pi\alpha(\mu_m + 2\beta_m)} + \frac{4\mu_m}{3\pi\alpha\beta_m}\right], \tag{7}$$

and

$$\beta = \mu\frac{3K + \mu}{3K + 4\mu}, \tag{8}$$

$$\zeta = \frac{\mu}{6}\frac{9K + 8\mu}{K + 2\mu}. \tag{9}$$

In the self-consistent approximation (O'Connell and Budiansky, 1974) one still uses the mathematical solution for the deformation of isolated inclusions, but the interaction of inclusions is approximated by replacing the background medium with the a priori unknown effective medium (P and Q are given above):

$$K^*(\phi) = K_m\,(1 - \phi P^*), \tag{10}$$

$$\mu^*(\phi) = \mu_m\,(1 - \phi Q^*), \tag{11}$$

Note, the self-consistent approximation for randomly oriented inclusions agrees with the first order corrections predicted by Hudson (1981).
The differential effective medium (DEM) theory models two-phase composites by incrementally adding inclusions of one phase to the matrix phase. The predictions can be expressed by two coupled linear differential equations with initial conditions $K^*(0) = K_m$ and $\mu^*(0) = \mu_m$ which can be solved numerically (Berryman, 1992):

$$(1 - \phi)\frac{d}{d\phi}[K^*(\phi)] = -K^*(\phi)P^*, \tag{12}$$

$$(1 - \phi)\frac{d}{d\phi}[\mu^*(\phi)] = -\mu^*(\phi)Q^*. \tag{13}$$

Norris (1985) have shown that the DEM is realizable and therefore is always consistent with the Hashin-Shtrikman upper and lower bounds (Hashin and Shtrikman, 1963).
The low aspect ratio of ellipsoidal cracks we used in our considerations makes it possible to compare the results with effective medium theories constructed only for (flat) disks. The difference between low aspect ratio ellipsoidal inclusions and disks does not significantly influence the predictions of the three theories discussed above (compare with Douma (1988)). Hence, we include in our comparison of theories the theory of non-interacting cracks (disks) of Kachanov (1992):

$$E^*(\rho) = E_m\left[1 + \frac{16(1 - \nu_m^2)(1 - 3\nu_m/10)}{9(1 - \nu_m/2)}\rho\right]^{-1}, \tag{14}$$

$$\mu^*(\rho) = \mu_m\left[1 + \frac{16(1 - \nu_m)(1 - \nu_m/5)}{9(1 - \nu_m/2)}\rho\right]^{-1}, \tag{15}$$

where ν_m is the Poisson ratio of the background material.

Intersecting cracks

In the effective medium theories presented above the fractures are modeled as ellipsoidal cavities. As mentioned by Schoenberg and Sayers (1995) real fractures do not resemble isolated voids in a solid matrix. Borehole pictures, examination of outcrops, and rock fractured in the laboratory all indicate that fractures have many points of contact along their length. Therefore we extend our numerical considerations to intersecting cracks. This is beyond the validity of most effective media theories.

For a random array of overlapping cracks it is possible to define a connectivity percolation threshold ρ_p. At this crack density the crack-network allows fluid flow through the fractured rock. In the literature we found two approaches with two substantially different predictions of this value for thin penny shaped cracks (disks):

$$\rho_p = 1.8/\pi^2 = 0.182 \text{ (Charlaix, 1986),} \tag{16}$$

$$\rho_p = 3.0/\pi^2 = 0.304 \text{ (Garboczi et al., 1995).} \tag{17}$$

The authors of the later paper are puzzled by the reason for this disagreement because the study of Charlaix (1986) does not reveal any obvious mistakes.
It is important to distinguish between the connectivity percolation threshold described above and the critical porosity (e.g. Nur (1992); Mukerji et al. (1995); Saenger and Shapiro (2002)) at which rocks lose rigidity and fall apart. The determination of the critical porosity (or critical crack density ρ_r) for randomly oriented and randomly distributed thin penny-shaped cracks has not been documented in the literature so far to our knowledge. But it is clear that the rigidity threshold characterized by ρ_r is much larger than the connectivity threshold ($\rho_r >> \rho_p$).

Fluid filled cracks

The "Kuster-Tuksöz formulation", the "Self-Consistent approximation" and the "Differential Effective Medium (DEM) theory" can be used also for fluid-filled cracks. For the exact analytical expressions we refer to the references given in the previous sections. Note, since the cavities are isolated with respect to flow, these approaches simulate the high frequency behavior of saturated rocks (the high frequency limit of the squirt model). This should not be confused with the fact that these theories are often termed low frequency theories as inclusions dimensions are assumed to be much smaller than a wavelength (Mavko et al., 1998).
If all cracks were connected an alternative method to predict effective moduli of fluid-filled fractured media would be the application of the Gassmann-equation (Gassmann, 1951):

$$\frac{K_{\text{sat}}}{K_0 - K_{\text{sat}}} = \frac{K_{\text{dry}}}{K_0 - K_{\text{dry}}} + \frac{K_{\text{fl}}}{\phi(K_0 - K_{\text{fl}})} \tag{18}$$

$$\mu_{\text{sat}} = \mu_{\text{dry}} \tag{19}$$

where

K_{dry}	effective bulk modulus of dry rock
K_{sat}	effective bulk modulus of the rock with pore fluid
K_0	bulk modulus of mineral making up rock
K_{fl}	effective bulk modulus of pore fluid
ϕ	porosity
μ_{dry}	effective shear modulus of dry rock
μ_{sat}	effective shear modulus of rock with pore fluid

Again, in this equation both phases, the fluid and the mineral, are assumed to be continuous. This is not the case for isolated penny-shaped cracks. However, we want to numerically clarify if the Gassmann-equation can be used for such cracks in the low-porosity limit.

Scattering attenuation

Among other theories Hudson (1981) presents the attenuation coefficient ($\gamma_p = \omega Q^{-1}/2v_p$, Q := quality factor) for the mean field of elastic waves in fractured media. For randomly oriented cracks (isotropic

distribution) the P-wave attenuation coefficient is given as:

$$\gamma_p = \frac{\omega}{v_s}\rho\left(\frac{\omega a}{v_p}\right)^3 \frac{4}{225\pi}\left[AU_1^2 + \frac{1}{2}\frac{v_p^5}{v_s^5}B(B-2)U_3^2\right] \quad (20)$$

$$A = \frac{3}{2} + \frac{v_s^5}{v_p^5} \quad (21)$$

$$B = 2 + \frac{15}{4}\frac{v_s}{v_p} - 10\frac{v_s^3}{v_p^3} + 8\frac{v_s^5}{v_p^5} \quad (22)$$

$$U_1 = \frac{16(\lambda+2\mu)}{3(3\lambda+4\mu)} \quad (23)$$

$$U_3 = \frac{4(\lambda+2\mu)}{3(\lambda+\mu)} \quad (24)$$

The isotropic background elastic moduli are λ and μ (Lamé parameters) while v_p and v_s denote the P- and S-wave velocity, respectively. The fourth power dependence on angular frequency ω is characteristic of Rayleigh scattering, which can only be observed if the wavelength is large compared to the dimension of the scatterers.

NUMERICAL EXPERIMENTS

The propagation of elastic waves is described by the elastodynamic wave equation (e.g. Aki and Richards (1980)):

$$\rho_g(\mathbf{r})\ddot{u}_i(\mathbf{r}) = (c_{ijkl}(\mathbf{r})u_{k,l}(\mathbf{r}))_{,j} + f_i(\mathbf{r}). \quad (25)$$

For modeling elastic waves at the position **r** with finite-differences, it is necessary to discretize the stiffness tensor c_{ijkl}, the (gravitational) density ρ_g, the displacement wave field u_i and the body force f_i on a grid.

Numerical setup

In order to test the different effective medium theories mentioned above we apply the so-called rotated staggered FD scheme to model wave propagation in fractured media (Saenger et al., 2000). Before comparing analytical predictions with numerical data it is necessary to clarify how accurate the numerical calculations are. After a detailed description of our modeling procedure we will consider possible sources of numerical errors.

We design a number of numerical elastic models (details can be found in Table 1) which include a region with a well known number of cracks and porosity. This fractured region (always from a depth of 173 gridpoints in the model) was filled at random with randomly oriented thin penny-shaped cracks. The implementation of the cracks on the 3D cubic FD grid is carried out by assigning crack properties to single neighboring gridpoints. The best possible representation of a 3D thin penny-shaped crack gives a rough disk-like inclusion (due to discretization) with a thickness of one gridpoint. For models with non-intersecting cracks the same procedure as in Davis and Knopoff (1995) and in Dahm and Becker (1998) is used: If two cracks intersected during random selection, the more recent crack was eliminated and a random choice was made again. In Figure 1 we can see a typical model. All models are always discretized with an interval of 0.0002m. In the homogeneous regions we set $v_p = 5100\ m/s$, $v_s = 2944\ m/s$ and $\rho_g = 2540\ kg/m^3$. For the dry penny-shaped cracks we set $v_p = 0\ m/s$, $v_s = 0\ m/s$ and $\rho_g = 0.0001\ kg/m^3$ which approximates vacuum. For the case of fluid-filled penny-shaped cracks we set $v_p = 1485\ m/s$, $v_s = 0\ m/s$ and $\rho_g = 1000\ kg/m^3$ which approximates water. It is important to note that we perform our modeling experiments with periodic boundary conditions in the two horizontal directions. For this reason our elastic models are generated also with this periodicity. Hence, it is possible for a single crack to start at the right side of the model and to end at its left side.

To obtain effective velocities in different models (with a different number of cracks) we apply a body force plane source at the top of the model. The plane wave generated in this way propagates through the fractured medium (see Figure 1). With two horizontal planes of receivers at the top and at the bottom,

No. (allocation number)	number of cracks	crack radius a [0.0002m]	size of cracked region $[(0.0002m)^3]$	total height of model [0.0002m]	porosity ϕ of the crack region	crack density ρ	N
1	20	31.5	400^3	805	0.0011	0.0098	1
2.1 - 2.3	40	31.5	400^3	805	0.0023	0.0195	3
3.1 - 3.3	80	31.5	400^3	805	0.0045	0.039	3
4.1 - 4.3	160	31.5	400^3	805	0.0090	0.078	3
5	240	31.5	400^3	805	0.0135	0.117	1
6.1 - 6.3	320	31.5	400^3	805	0.0180	0.156	3
7.1 - 7.3	60	31.5	$300^2 \times 400$	1305	0.0060	0.052	3
8.1 - 8.3	30	41.5	$250^2 \times 500$	1305	0.0060	0.069	3
9.1x - 9.3x	40	31.5	400^3	805	0.0023	0.0195	3
10.1x - 10.3x	80	31.5	400^3	805	0.0044	0.039	3
11.1x - 11.3x	160	31.5	400^3	805	0.0089	0.078	3
12.1x - 12.3x	320	31.5	400^3	805	0.0179	0.156	3
13x	700	31.5	400^3	805	0.038	0.342	1
14x	1000	31.5	400^3	805	0.054	0.488	1
15x	1200	31.5	400^3	805	0.065	0.585	1
16x	2000	31.5	400^3	805	0.106	0.977	1

Table 1: Crack models for numerical calculations. The models with an x attached to its number have intersecting cracks. Note, $0.0002m$ is the size of grid spacing and N denotes the number of model realizations. The cracks can be fluid-filled or empty.

it is possible to measure the time-delay of the mean peak amplitude of the plane wave caused by the inhomogeneous region. With the time-delay one can estimate the effective velocity. Additionally, the attenuation of the plane wave can be studied. The source wavelet in our experiments is always the first derivative of a Gaussian with a dominant frequency of $8 * 10^5\ 1/s$ and with a time increment of $\Delta t = 2.1 * 10^{-8} s$. The resulting power spectrum of the plane P-wave is shown in Figure 8. Due to the size of the models we have to use large-scale computers (e.g. CRAY T3E) with a MPI implementation of our modeling software. In fact, the size-restriction of our models is mainly due to computational restrictions in memory and CPU-time.
Similar to Garboczi and Berryman (2001), Ursenbach (2001) and Arns (2002) we detect three main sources of error in our numerical calculations: (1) finite size effect, (2) digital resolution and (3) statistical variation. Two other sources of error, specific for finite-difference solutions of the elastodynamic wave equation, are: (4) numerical dispersion and (5) the general modeling accuracy for high-contrast inclusions.

(1) Finite size errors result from having a sample (fractured region) of finite size, where the largest length scales of inclusions are of the order of the sample size. Samples at this scale can be not representative any more, and the numerical data becomes noisy. Experience with many previous results (Garboczi and Berryman, 2001; Saenger and Shapiro, 2002) has shown that having the ratio of the sample size to the diameter of the penny-shaped crack to be about 7 makes finite size errors negligible.

(2) The digital resolution error comes from using a rectangular finite-difference grid. The crack geometries have to be represented on this given grid-structure. We observe only very small variations among the different crack sizes we have used (shown below). An important argument, that the digital resolution error is below an acceptable level, is the fact that for low crack densities all theories and numerical results are in a good agreement. However, this error is the most critical error in our numerical measurements (and in the similar studies of Garboczi and Berryman (2001), Ursenbach (2001) and Arns (2002)).

(3) The statistical variation error comes about because the models under consideration are random ones. For a given crack density, there are many ways in which the cracks might be randomly arranged. Each arrangement will have somewhat different effective elastic moduli, in general. The error bar in our numerical results denotes the standard deviation for different model realizations. It can be observed that this deviation is always very small.

(4) In order to reduce the dispersion error of the FD simulations we use only 54% of the allowed maximum time increment ($\gamma = 0.54\ \gamma_{max}$; see Saenger et al. (2000)). All computations are performed with second order spatial FD operators and with a second order time update. The number of grid points

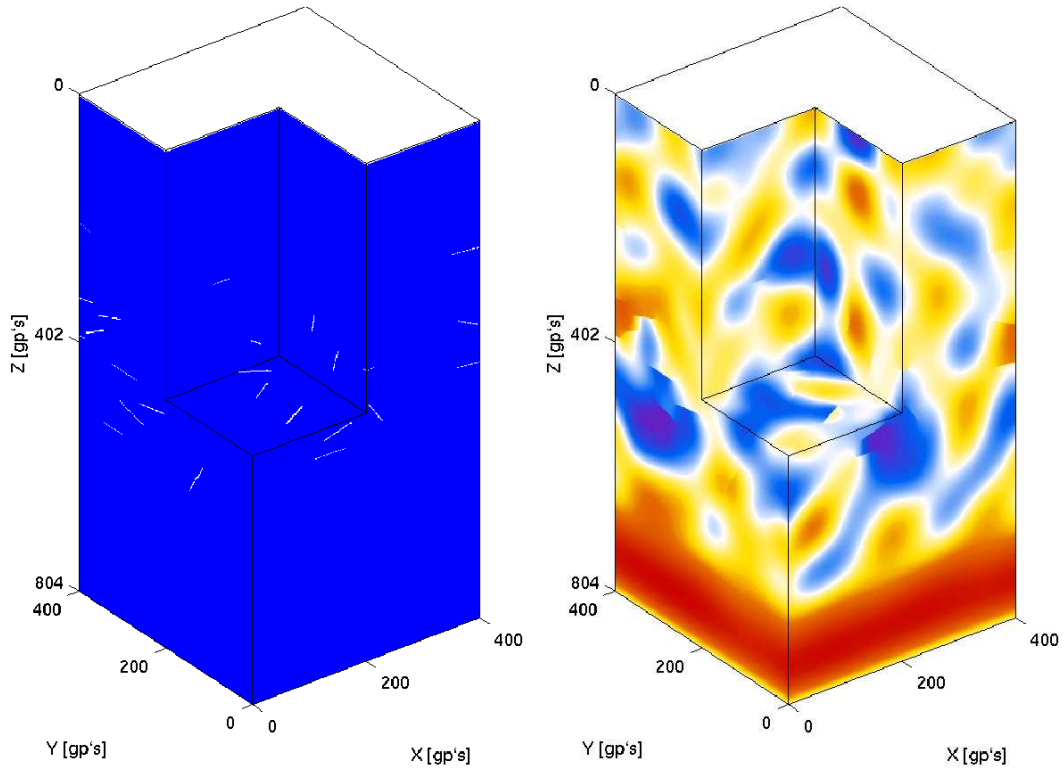

Figure 1: Left: A typical 3D fractured model with non-intersecting penny-shaped cracks (with radius $r = 31.5$ grid points) used for the numerical experiments. We introduce a cracked region ($400 \times 400 \times 400$ grid points) in a homogeneous material. At the top we place a small strip of vacuum. This is advantageous for applying a body force plane source with the rotated staggered grid. **Right**: A z-displacement-snapshot of a plane *P*-wave propagating through the fractured 3D model. We use a non-linear color scale to emphasize the scattered wavefield. The visible discontinuities of the wavefield correspond to the crack locations (compare with Figure on the left).

per wavelength N_λ is equal or greater than 100. Therefore, with this configuration our measurements are for a homogeneous model with a crack density of $\rho = 0$ a velocity of $v_p = 5102.91 ms^{-1}$ (relative error: 0.057%) and $v_s = 2943.62 ms^{-1}$ (relative error: 0.004%).

(5) Krüger et al. (2002) studied the numerical accuracy of the rotated staggered grid (RSG) for high contrast inclusions. They compared the analytically and numerically derived power spectra and seismograms of *SH*-wave diffraction by a finite plane crack. Both approaches, the analytical solution of Sánchez-Sesma and Iturrarán-Viveros (2001) and the numerical solution using the RSG, show an excellent correspondence. A remarkable aspect is that for inclined cracks the numerical solution is still correct, even though the crack is discretisized on a grid and does not have a perfect plane surface.

Numerical results for effective *P*- and *S*-wave velocities for non-intersecting dry penny-shaped cracks

Our numerical results for penny-shaped dry cracks are depicted by dots in Figure 2 and Figure 3. We show the relative decrease of the normalized effective *P*- and *S*-wave velocity in dependence of the crack density ρ. For the case of non-intersecting cracks we use models No. 1, 2.1-2.3, 3.1-3.3, 4.1-4.3, 6.1-6.3, 7.1-7.3, 8.1-8.3 for *P*-waves and models No. 3.1, 4.1, 5, 6.1-6.2 for *S*- waves (Table 1). For comparison, the predictions of the four theories described in previous Section are also shown. Note, it is not useful to study higher crack densities than the connectivity percolation threshold (Eq. 16 and 17) for non-intersecting cracks. For those high crack densities it is problematic to generate high order statistical independent crack models (one has to remove too many cracks in the model build-up process).

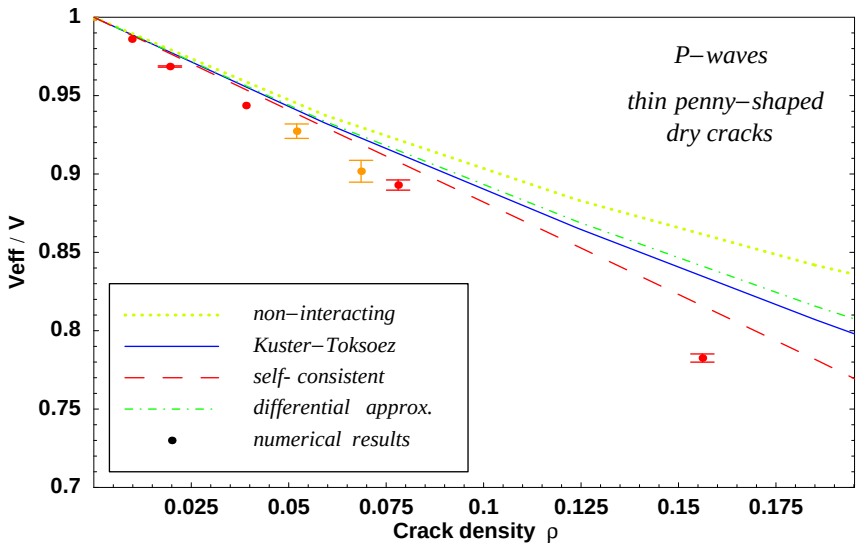

Figure 2: Normalized effective velocity of compressional (*P*-) waves versus crack density ρ of penny-shaped cracks. Dots: Numerical results of this study. The error bars denote the standard deviation for different model realizations (see Table 1). The dotted and the dashed-dotted line are predicted by the theory of non-interacting cracks and the differential effective medium (DEM) theory, respectively. The solid line is the prediction by the Kuster-Toksöz approach and the dashed line is due to the self consistent approximation.

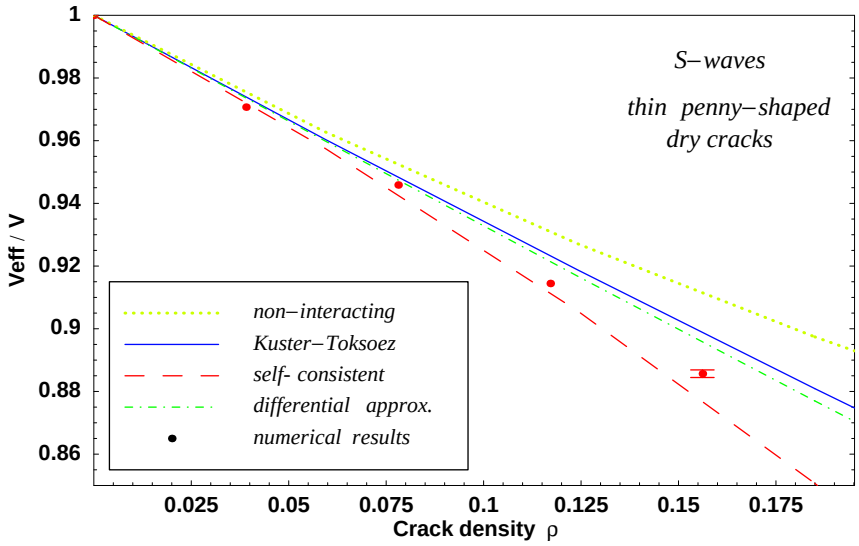

Figure 3: Same as Fig. 2 for shear (*S*-) waves

The first conclusion is that none of the theories provides precise results for relatively high crack densities. Overall, they tend to underestimate the effect of velocity-reduction by empty cracks. This can be particularly observed for the theory of non-interacting cracks by Kachanov (1992). The best match to the numerical estimates gives the self-consistent approximation (O'Connell and Budiansky, 1974). This is most significant for the effective *P*-wave velocities. A comparison with experimental data described in a

recent review of Hudson's model for cracked media (Hudson et al., 2001) provides a similar conclusion. As mentioned above the self-consistent approximation for randomly oriented inclusions agrees with the first order corrections predicted by Hudson (1981).
At a first glance our 3D results seem to be in conflict with the numerical results of 2D fractured media presented in Saenger and Shapiro (2002). They support in contrast to the 3D results the *modified self-consistent theory* (similar to DEM) for relative high crack densities. However, a closer look to the 2D results (Fig. 2 of Saenger and Shapiro (2002)) shows that at slightly higher crack densities (in a middle range) the self-consistent theory and the numerical results have also a good agreement. A general underestimation of velocity-reduction by empty cracks by the 2D theory for non-interacting cracks by Kachanov (1992) can be observed, too. Therefore, we assert that the 2D and 3D results complement each other.

Numerical results for effective *P*-wave velocities for intersecting dry penny-shaped cracks

For intersecting cracks it is unproblematic to generate statistically independent models with high crack densities because it is not necessary to eliminate intersecting cracks in the random generation process. The details of the used models No. 9.1x-9.3x, 10.1x-10.3x, 11.1x-11.3x, 12.1x-12.3x, 13x, 14x, 15x, 16x with intersecting cracks can be found in Table 1. The 3D numerical results for the normalized effective *P*-wave velocities for thin penny-shaped dry cracks are shown in Figure 4.

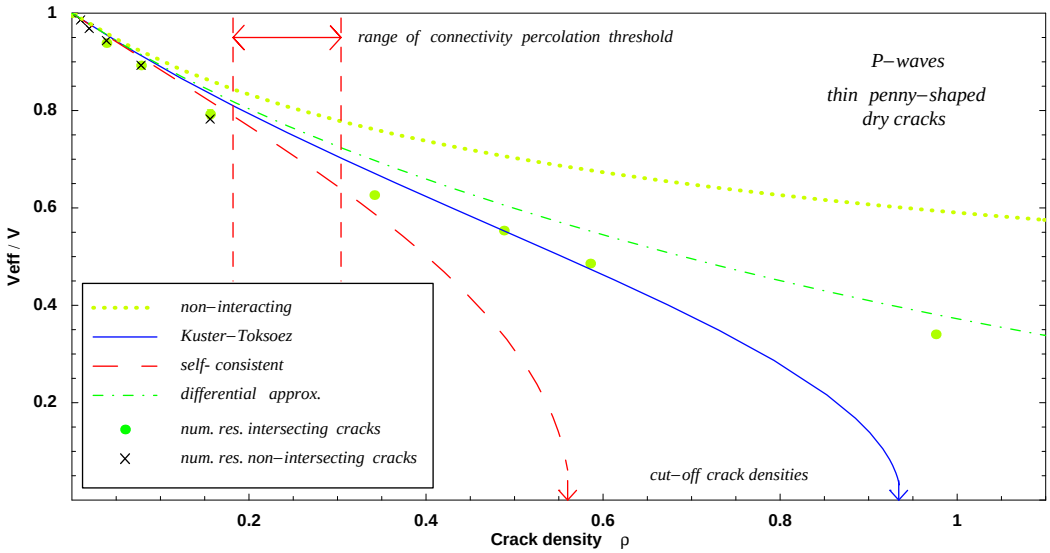

Figure 4: Normalized effective velocity of compressional (*P*-) waves versus crack density ρ of **intersecting** and non-intersecting penny-shaped cracks. **Dots**: Numerical results for **intersecting** cracks. Crosses: Numerical results for non-intersecting cracks. The dotted and the dashed-dotted lines are predicted by the theory of non-interacting cracks and the differential effective medium (DEM) theory, respectively. The solid line is the prediction by the Kuster-Toksöz approach and the dashed line represents the self consistent approximation. The cut-off crack density of the self-consistent approximation and the Kuster-Toksöz approach is $\rho_{cf} = 0.56$ and $\rho_{cf} = 0.93$, respectively. The arrow displays the range of the connectivity percolation threshold (see Section II).

It is interesting to observe that the connectivity percolation threshold (Eq. 16 and 17) cannot be clearly detected in the seismic signatures of the numerical experiments. The difference of effective velocities for intersecting or non-intersecting cracks is not significant for crack densities below this range. Although the effective medium theories described above are not derived for intersecting cracks we test their applicability for such media. Therefore, for comparison the predictions of this theories are also depicted in Figure 4. For the self-consistent approximation and the Kuster-Toksöz approach one can estimate an unphysical cut-off crack density ρ_{cf}. At this crack density the theories predict an effective velocity of zero for *P*- and *S*-waves.

This cut-off crack density is not related to the rigidity percolation threshold ρ_r.
Again, as for non-intersecting cracks, none of the theories provide precise results for high crack densities. However, the best fit between numerical results for high crack densities and the theoretical predictions gives the DEM theory. Along with the assumption $\rho_r >> \rho_p$ this is again consistent with the findings of Saenger and Shapiro (2002).

Numerical results for effective *P*- and *S*-wave velocities for non-intersecting fluid-filled penny-shaped cracks

For the calculations of effects of penny-shaped fluid-filled cracks we have used models No. 3.1-3.3, 4.1, 6.1-6.3 for *P*-waves and No. 3.1, 4.1, 5, 6.1-6.2 for *S*-waves (Table 1). The relative decrease of the normalized effective *P*- and *S*-wave velocity in dependence of the crack density ρ is shown in Figure 5 and 6. For comparison, the three effective medium theories for isolated fluid-filled cracks discussed in Section II are also displayed.

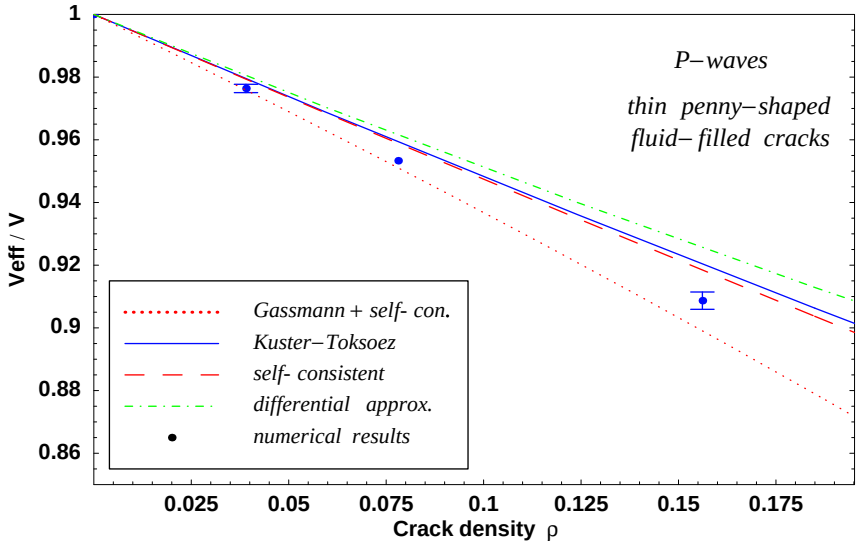

Figure 5: Normalized effective velocity of compressional (*P*-) waves versus crack density ρ of fluid-filled non-intersecting penny-shaped cracks. Dots: Numerical results of this study. The error bar denotes the standard deviation for different model realizations (see Table 1). The dashed-dotted line is predicted by the differential effective medium (DEM) theory. The solid line is the prediction by the Kuster-Toksöz approach and the dashed line is due to the self consistent approximation. The dotted line is found by taking the self-consistent effective moduli for dry cracks, and saturating them with the Gassman-equation.

From the numerical point of view it is not possible to distinguish non-ambiguous which effective medium theory gives the best prediction. The differences of the theoretical approaches for the investigated crack densities are very low. Once again, as for empty cracks, one can detect the trend that the theories underestimate the effect of velocity-reduction caused by the inclusions. There is only a slight indication that the self-consistent approach is superior to other theories.
Additionally, another interesting fact can be observed: If one combines the self-consistent theory to estimate the dry rock moduli with the Gassmann-equation it is possible to predict the low-frequency behavior of the Squirt-model for fluid saturated rocks (Mavko et al., 1998). As discussed in section II this is not a valid assumption for our models used for the numerical considerations. This mismatch can clearly be detected in the numerical *S*-wave data (Figure 6). This is an additional indication for the sensitivity of our numerical validation of effective medium theories.
Our numerical setup enables us to study 3D fractured media with exact the same crack positions for fluid-filled and for empty cracks (i.e. the dry rock frame is exactly the same in both simulations). Therefore we

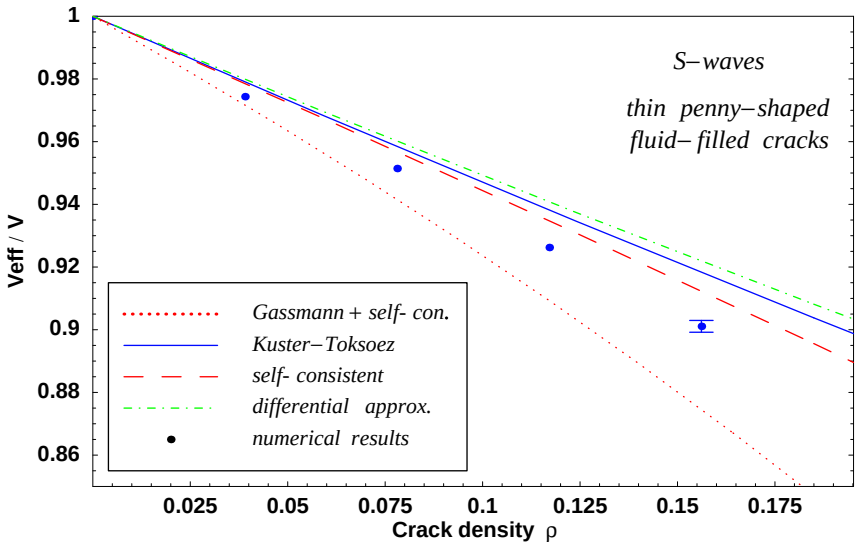

Figure 6: Same as Fig. 5 for shear (*S*-) waves.

can test the applicability of the Gassmann-equation for our 3D fractured materials without any additional effective medium theory. The calculated normalized effective shear moduli μ^* for fluid-filled and for empty cracks are compared in Figure 7. There is a significant difference between both moduli below the range of the connectivity percolation threshold. This bring us to the conclusion that the Gassmann-equation cannot be applied to isolated fluid-filled cracks even with a low porosity in the used models. From a practical point of view this has the following consequence: If one applies the Gassmann-equation one has to distinguish between the isolated fraction and the continuous fraction of the fluid. The isolated fluid fraction should be considered as a part of the 'dry' rock frame.

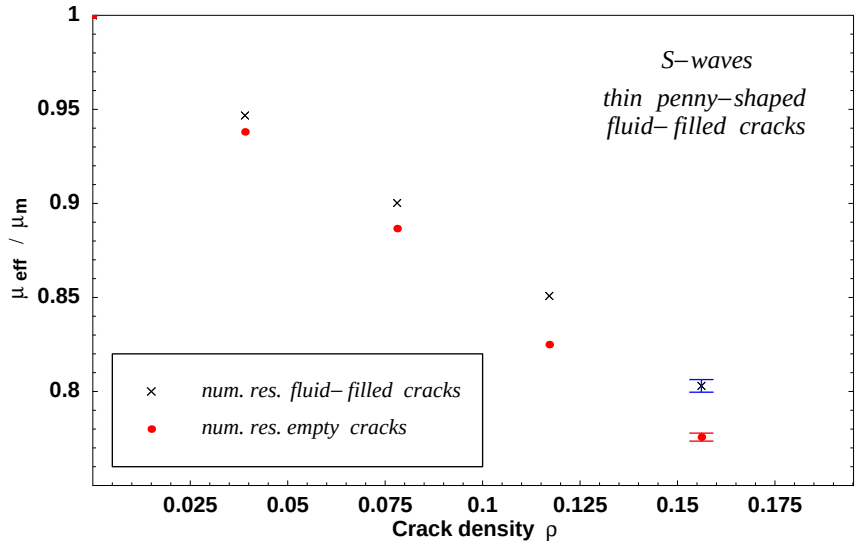

Figure 7: Normalized effective shear moduli μ^* calculated from the effective shear wave velocities depicted in Figure 3 and Figure 6. The dry rock frame is exactly the same for the used models with empty (depicted with dots) and fluid-filled cracks (depicted with crosses).

Scattering attenuation for non-intersecting dry penny-shaped cracks

In this section we consider the scattering attenuation coefficient (Eq. 20) predicted by Hudson (1981). In contrast to the velocity considerations we are interested to record the complete transmitted plane wave. From the numerical point of view it is necessary to modify the standard model size used so far. Therefore we use the models 7.1-7.3 with an extended total height (Table 1).
The frequency-depended relative attenuation A is calculated by dividing the Fourier transform of the transmitted meanfield of the plane wave through the power spectrum of the incident plane wave. Additionally, the attenuation coefficient γ is estimated by using $\gamma = -(\ln A)/L$ (L denotes the length of the travel path). A comparison of the results of the Hudson-approach and our numerical results is shown in Figure 8. We observe a very good agreement. The systematic oscillations in the numerical results can be explained with the relatively short travel path through the fractured media and internal oscillations. Note, the observed typical Rayleigh scattering is an additional indication that our simulations represent the long wavelength limit.

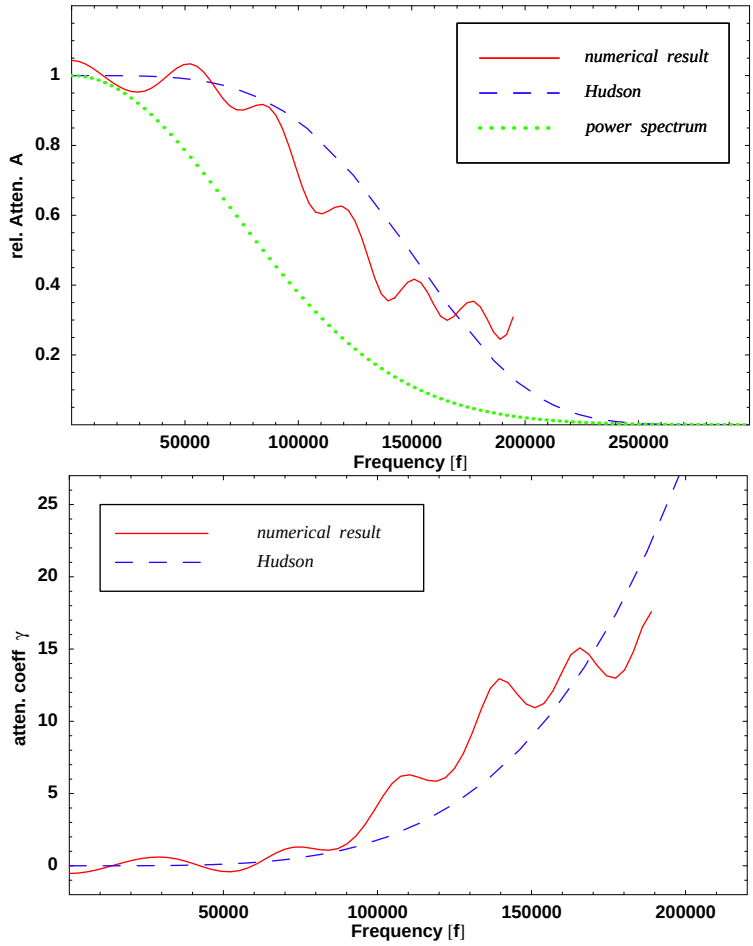

Figure 8: Top: The solid line displays the relation between power spectra of transmitted (through the region with empty penny-shaped cracks) and incident signal of the P-wave. The dashed line shows the same quantity predicted by Hudson (1981) using Eq. 20. The dotted line is the normalized power spectrum of the generated plane P-wave of the simulation. The frequency corresponding to the diameter of the cracks is $f = v_p/(2a) = 425000Hz$. The crack density of the corresponding three models is $\rho = 0.045$. **Bottom:** Same as Top, but now the attenuation coefficient γ_p is depicted. The fourth power dependence on frequency f of Rayleigh scattering can be clearly observed.

CONCLUSIONS

Finite-difference modeling of the elastodynamic wave equation is very fast and accurate. We use the rotated staggered FD grid to calculate elastic wave propagation in fractured media. Our numerical modeling of elastic properties of dry and fluid-saturated rock skeletons can be considered as an efficient and well controlled computer experiment. In this paper we consider 3D isotropic fractured media with ellipsoidal inclusions.

We have numerically tested effective velocity predictions of different theoretical approaches: The theory for non-interacting cracks, the Kuster-Toksöz approach, the self-consistent theory, the differential effective medium (DEM) theory and the Gassmann-equation. For non-intersecting dry and fluid-filled penny-shaped cracks at slightly higher crack densities (below the connectivity percolation threshold for intersecting cracks) the self consistent theory is most successful in predicting effective velocities for *P*- and *S*-waves. The Gassmann-equation cannot be applied to isolated fluid-filled cracks, even not in the case of a low porosity.

The more realistic assumption (with respect to natural rocks) of intersecting cracks is not included in the effective medium theories described above. However, below the range of the connectivity percolation threshold the difference of effective velocities for intersecting and non-intersecting cracks is negligible. For crack densities beyond this range the DEM (not derived for intersecting cracks) is superior to apply.

Additionally, we have studied scattering attenuation of the meanfield. The attenuation coefficient predicted by Hudson (1981) can be used for ellipsoidal high contrast inclusions.

ACKNOWLEDGEMENTS

This work was kindly supported by the sponsors of the *Wave Inversion Technology (WIT) Consortium*, Berlin, Germany.

REFERENCES

Aki, K. and Richards, P. G. (1980). *Quantitative Seismology, Theory and Methods*. W.H. Freeman and Comp., San Fransisco.

Arns, C. H. (2002). *The influence of morphology on physical properties of reservoir rocks*. PhD thesis, University of New South Wales.

Berryman, J. G. (1992). Single-scattering approximations for coefficients in biot's equations of poroelasticity. *J. Acoust. Soc. Amer.*, 91:551–571.

Charlaix, E. (1986). Percolation threshold of a random array of discs: a numerical simulation. *J. Phys. A*, 19:L533–L536.

Cheng, C. H. (1993). Crack models for a transversely isotropic medium. *Journal of Geophysical Research*, 98(B1):675–684.

Dahm, T. and Becker, T. (1998). On the elastic and viscous properties of media containing strongly interacting in-plane cracks. *Pure Appl. Geophys.*, 151:1–16.

Davis, P. M. and Knopoff, L. (1995). The elastic modulus of media containing strongly interacting antiplane cracks. *J. Geophys. Res.*, 100:18.253–18.258.

Douma, J. (1988). The effect of the aspect ratio on crack-induced anisotrophy. *Geophysical Prospecting*, 36:614–632.

Garboczi, E. J. and Berryman, J. G. (2001). Elastic moduli of a material containing composite inclusions: Effective medium theory and finite element computations. *Mechanics of Materials*, 33:455–470.

Garboczi, E. J. and Day, A. R. (1995). Algorithm for computing the effective linear elastic properties of heterogeneous materials: Three-dimensional results for composites with equal phase poisson ratios. *J. Mech. Phys. Solids*, 43:1349–1362.

Garboczi, E. J., Snyder, K. A., Douglas, J. F., and Thorpe, M. F. (1995). Geometrical percolation threshold of overlapping ellipsoids. *Physical Review E*, 52(1):819–828.

Gassmann, F. (1951). Über die Elastizität poröser Medien. *Vier. der Natur Gesellschaft*, 96:1–23.

Hashin, Z. and Shtrikman, S. (1963). A variational approach to the elastic behavior of multiphase materials. *J. Mech. Phys. Solids*, 11:127–140.

Hudson, J. A. (1981). Wave speeds and attenuation of elastic waves in material containing cracks. *Geophys. J. Royal Astronom. Soc.*, 64:133–150.

Hudson, J. A., Pointer, T., and Liu, E. (2001). Effective-medium theories for fluid-saturated materials with aligned cracks. *Geophysical Prospecting*, 49:509–522.

Kachanov, M. (1992). Effective elastic properties of cracked solids: critical review of some basic concepts. *Appl. Mech. Rev.*, 45(8):304–335.

Kelly, K. R., Ward, R. W., Treitel, S., and Alford, R. M. (1976). Synthetic seismograms: A finite-difference approach. *Geophysics*, 41:2–27.

Krüger, O. S., Saenger, E. H., and Shapiro, S. (2002). *Simulation of the diffraction by single cracks: an accuracy study*, page SM P1.2. 72st Ann. Internat. Mtg, Soc. of Expl. Geophys.

Kuster, G. T. and Toksöz, M. N. (1974). Velocity and attenuation of seismic waves in two-phase media: Part I: Theoretical formulations. *Geophysics*, 39:587–606.

Mavko, G., Mukerji, T., and Dvorkin, J. (1998). *The Rock Physics Handbook*. Cambridge University Press, Cambridge.

Mukerji, T., Berryman, J., Mavko, G., and Berge, P. (1995). Differential effective medium modeling of rock elastic moduli with critical porosity constraints. *Geophysical Research Letters*, 22(5):555–558.

Norris, A. N. (1985). A differential scheme for the effective moduli of composites. *Mech. of Mater.*, 4:1–16.

Nur, A. (1992). Critical porosity and the seismic velocities in rocks (abstract). *EOS Trans. AGU*, 73:66.

O'Connell, R. J. and Budiansky, B. (1974). Seismic velocities in dry and saturated cracked solids. *J. Geophys. Res.*, 79:5412–5426.

Saenger, E. H., Gold, N., and Shapiro, S. A. (2000). Modeling the propagation of elastic waves using a modified finite-difference grid. *Wave Motion*, 31(1):77–92.

Saenger, E. H. and Shapiro, S. A. (2002). Effective velocities in fractured media: A numerical study using the rotated staggered finite-difference grid. *Geophysical Prospecting*, 50(2):183–194.

Sánchez-Sesma, F. J. and Iturrarán-Viveros, U. (2001). Scattering and diffraction of SH waves by a finite crack: an analytical solution. *Geophys. J. Int.*, 145:749–758.

Schoenberg, M. and Sayers, C. M. (1995). Seismic anisotropy of fractured rock. *Geophysics*, 60(01):204–211.

Ursenbach, C. P. (2001). *Simulation of elastic moduli of porous media*, pages 1704–1707. 71st Ann. Internat. Mtg.,Soc. of Expl. Geophys.

Virieux, J. (1986). Velocity-stress finite-difference method. *Geophysics*, 51:889–901.